

Research Article

Radiant Exposure Fractal Dimension for Characterizing Shajara Reservoirs of the Permo-Carboniferous Shajara Formation

Khalid Elyas Mohamed Elameen Alkhidir

Department of Petroleum and Natural Gas Engineering, College of Engineering,
King Saud University, Saudi Arabia.

*Corresponding author's e-mail: kalkhidir@ksu.edu.sa

Abstract

The quality and assessment of a reservoir can be documented in details by the application of radiant exposure. This research aims to calculate fractal dimension from the relationship among radiant exposure, maximum Radiant exposure and wetting phase saturation and to approve it by the fractal dimension derived from the relationship among capillary pressure and wetting phase saturation. Two equations for calculating the fractal dimensions have been employed. The first one describes the functional relationship between wetting phase saturation, Radiant exposure, maximum Radiant exposure and fractal dimension. The second equation implies to the wetting phase saturation as a function of capillary pressure and the fractal dimension. Two procedures for obtaining the fractal dimension have been utilized. The first procedure was done by plotting the logarithm of the ratio between Radiant exposure and maximum Radiant exposure versus logarithm wetting phase saturation. The slope of the first procedure = $3 - D_f$ (fractal dimension). The second procedure for obtaining the fractal dimension was determined by plotting the logarithm of capillary pressure versus the logarithm of wetting phase saturation. The slope of the second procedure = $D_f - 3$. On the basis of the obtained results of the fabricated stratigraphic column and the attained values of the fractal dimension, the sandstones of the Shajara reservoirs of the Shajara Formation were divided here into three units.

Keywords: Shajara Reservoirs; Shajara Formation; Radiant exposure fractal dimension; Capillary pressure fractal dimension.

Introduction

Seismo electric effects related to electro kinetic potential, dielectric permittivity, pressure gradient, fluid viscosity, and electric conductivity was first reported by [1]. Capillary pressure follows the scaling law at low wetting phase saturation was reported by [2]. Seismo electric phenomenon by considering electro kinetic coupling coefficient as a function of effective charge density, permeability, fluid viscosity and electric conductivity was reported by [3]. The magnitude of seismo electric current depends on porosity, pore size, zeta potential of the pore surfaces, and elastic properties of the matrix was investigated by [4]. The tangent of the ratio of converted electric field to pressure is approximately in inverse proportion to permeability was studied by [5].

Permeability inversion from seismoelectric log at low frequency was studied by [6]. They reported that, the tangent of the

ratio among electric excitation intensity and pressure field is a function of porosity, fluid viscosity, frequency, tortuosity, fluid density and Dracy permeability. A decrease of seismo electric frequencies with increasing water content was reported by [7]. An increase of seismo electric transfer function with increasing water saturation was studied by [8]. An increase of dynamic seismo electric transfer function with decreasing fluid conductivity was described by [9]. The amplitude of seismo electric signal increases with increasing permeability which means that the seismo electric effects are directly related to the permeability and can be used to study the permeability of the reservoir was illustrated by [10].

Seismo electric coupling is frequency dependent and decreases exponentially when frequency increases was demonstrated by [11]. An increase of permeability with increasing pressure head and bubble pressure fractal

dimension was reported by [12,13]. An increase of geometric relaxation time of induced polarization fractal dimension with permeability increasing and grain size was described by [14,15].

Materials and methods

Sandstone samples were collected from the surface type section of the Permo-Carboniferous Shajara Formation, latitude 26° 52' 17.4", longitude 43° 36' 18". (Figure 1). Porosity was measured on collected samples using mercury intrusion Porosimetry and permeability was derived from capillary pressure data. The purpose of this paper is to obtain Radiant exposure fractal dimension and to confirm it by capillary pressure fractal dimension. The fractal dimension of the first procedure is determined from the positive slope of the plot of logarithm of the ratio of Radiant exposure to maximum Radiant exposure $\log(H_e^{1/4}/H_{e_{max}}^{1/4})$ versus \log wetting phase saturation ($\log(S_w)$). Whereas the fractal dimension of the second procedure is determined from the negative slope of the plot of logarithm of \log capillary pressure ($\log P_c$) versus \log wetting phase saturation ($\log(S_w)$).

The radiant exposure can be scaled as eq. (1)

$$S_w = \left[\frac{H_e^{1/4}}{H_{emex}^{1/4}} \right]^{[3-Df]} \tag{1}$$

Where S_w the water saturation, H_e the radiant exposure in Joule / square meter, H_{emex} the maximum radiant exposure in Joule / square meter.

Eq. (1) can be proofed from

$$H_e = \left[\frac{Q_e}{A} \right] \tag{2}$$

Where H_e the radiant exposure in Joule /square meter, Q_e the radiant energy in joule, A the area in square meter

The radiant energy can be scaled as eq. (3).

$$Q_e = q * v \tag{3}$$

Where Q_e the radiant energy in joule, q the electric charge in coulomb, v the electric potential in volt

Insert eq. (3) into eq. (2)

$$H_e = \left[\frac{q * v}{A} \right] \tag{4}$$

The potential can be scaled as eq. (5)

$$v = E * k \tag{5}$$

Where v the electric potential in volt, E the electric field in volt, k the distance in meter

Insert eq. (5) into eq. (4).

$$H_e = \left[\frac{q * E * k}{A} \right] \tag{6}$$

The electric field can be scaled as eq. (7).

$$E = \left[\frac{V}{CEK} \right] \tag{7}$$

Where E the electric field in volt / meter, V the velocity of flow in meter /second, CEK the electro kinetic coefficient in ampere / pascal * meter

Insert eq. (7) into eq. (6).

$$H_e = \left[\frac{q * V * k}{A * CEK} \right] \tag{8}$$

The velocity of flow can be scaled as eq. (9).

$$v = \left[\frac{Q}{A} \right] \tag{9}$$

Where V the velocity in meter / second, Q the flow rate in cubic meter / second, A the area in square meter

Insert eq. (9) into eq. (8)

$$H_e = \left[\frac{q * Q * k}{A * CEK * A} \right] \tag{10}$$

The flow rate can be scaled as eq. (11)

$$Q = \left[\frac{3.14 * r^4 * \Delta P}{8 * \mu * L} \right] \tag{11}$$

Where Q the flow rate in cubic meter / second, r the pore radius in meter, ΔP the difference in pressure in pascal, μ the fluid viscosity in pascal * second, L the capillary length in meter

Insert eq. (11) into equation eq. (10).

$$H_e = \left[\frac{q * 3.14 * r^4 * \Delta P * k}{A * CEK * A * 8 * \mu * L} \right] \tag{12}$$

The maximum pore radius can be scaled as

$$H_{e_{max}} = \left[\frac{q * 3.14 * r_{max}^4 * \Delta P * k}{A * CEK * A * 8 * \mu * L} \right] \tag{13}$$

Divide eq. (12) by eq. (13).

$$\left[\frac{H_e}{H_{e_{max}}} \right] = \left[\frac{\left[\frac{q * 3.14 * r^4 * \Delta P * k}{A * CEK * A * 8 * \mu * L} \right]}{\left[\frac{q * 3.14 * r_{max}^4 * \Delta P * k}{A * CEK * A * 8 * \mu * L} \right]} \right] \quad 14$$

Eq. (14) after simplification will become eq. (15).

$$\left[\frac{H_e}{H_{e_{max}}} \right] = \left[\frac{r^4}{r_{max}^4} \right] \quad 15$$

Take the fourth root of eq. (15).

$$\sqrt[4]{\left[\frac{H_e}{H_{e_{max}}} \right]} = \sqrt[4]{\left[\frac{r^4}{r_{max}^4} \right]} \quad 16$$

Eq. (16) after simplification will become eq. (17).

$$\left[\frac{H_e^{\frac{1}{4}}}{H_{e_{max}}^{\frac{1}{4}}} \right] = \left[\frac{r}{r_{max}} \right] \quad 17$$

Take the logarithm of eq. (17).

$$\log \left[\frac{H_e^{\frac{1}{4}}}{H_{e_{max}}^{\frac{1}{4}}} \right] = \log \left[\frac{r}{r_{max}} \right] \quad 18$$

$$\text{But; } \log \left[\frac{r}{r_{max}} \right] = \left[\frac{\log Sw}{3 - Df} \right] \quad 19$$

Insert eq. (19) into eq. (18).

$$\left[\frac{\log Sw}{3 - Df} \right] = \log \left[\frac{H_e^{\frac{1}{4}}}{H_{e_{max}}^{\frac{1}{4}}} \right] \quad 20$$

Eq. (20) after log removal will become

$$Sw = \left[\frac{H_e^{\frac{1}{4}}}{H_{e_{max}}^{\frac{1}{4}}} \right]^{[3 - Df]} \quad 21$$

Eq. (21) the proof of eq. (1) which relates the water saturation, radiant exposure, maximum radiant exposure, and the fractal dimension

The capillary pressure can be scaled as eq. (22)

$$Sw = [Df - 3] * Pc * \text{constant} \quad 22$$

Where Sw the water saturation, Pc the capillary pressure and Df the fractal dimension.

Results and discussion

Based on field observation the Shajara Reservoirs of the Permo-Carboniferous Shajara Formation were divided here into three units as described in Figure1. These units from bottom to top are: Lower Shajara Reservoir, Middle Shajara reservoir, and Upper Shajara Reservoir. Their attained results of the Radiant exposure fractal dimension and capillary pressure fractal dimension are shown in Table 1.

Table 1. Petrophysical model showing the three Shajara Reservoir Units with their corresponding values of Radiant exposure fractal dimension and capillary pressure fractal dimension

Formation	Reservoir	Sample	Porosity %	k (md)	Positive slope of the first procedure Slope=3-Df	Negative slope of the second procedure Slope=Df-3	Radiant exposure fractal dimension	Capillary pressure fractal dimension
Permo-Carboniferous Shajara Formation	Upper Shajara Reservoir	SJ13	25	973	0.2128	-0.2128	2.7872	2.7872
		SJ12	28	1440	0.2141	-0.2141	2.7859	2.7859
		SJ11	36	1197	0.2414	-0.2414	2.7586	2.7586
	Middle Shajara Reservoir	SJ9	31	1394	0.2214	-0.2214	2.7786	2.7786
		SJ8	32	1344	0.2248	-0.2248	2.7752	2.7752
		SJ7	35	1472	0.2317	-0.2317	2.7683	2.7683
	Lower Shajara Reservoir	SJ4	30	176	0.3157	-0.3157	2.6843	2.6843
		SJ3	34	56	0.5621	-0.5621	2.4379	2.4379
		SJ2	35	1955	0.2252	-0.2252	2.7748	2.7748
		SJ1	29	1680	0.2141	-0.2141	2.7859	2.7859

Based on the achieved results it was found that the Radiant exposure fractal dimension is equal to the capillary pressure fractal dimension. The maximum value of the fractal dimension was found to be 2.7872 allocated to sample SJ13 from the Upper Shajara

Reservoir as verified in Table 1. Whereas the minimum value of the fractal dimension 2.4379 was reported from sample SJ3 from the Lower Shajara reservoir as shown in Table1. The Radiant exposure fractal dimension and capillary pressure fractal dimension were detected to

increase with increasing permeability as proofed in Table 1 owing to the possibility of having interconnected channels.

The Lower Shajara reservoir was symbolized by six sandstone samples (Figure 1), four of which label as SJ1, SJ2, SJ3 and SJ4 were carefully chosen for capillary pressure measurement as proven in Table 1. Their positive slopes of the first procedure log of the Radiant exposure to maximum Radiant exposure versus log wetting phase saturation (Sw) and negative slopes of the second procedure log capillary pressure (Pc) versus log wetting phase saturation (Sw) are clarified in Figure 2, Figure 3, Figure 4,

Figure 5 and Table 1. Their Radiant exposure fractal dimension and capillary pressure fractal dimension values are revealed in Table 1. As we proceed from sample SJ2 to SJ3 a pronounced reduction in permeability due to compaction was described from 1955 md to 56 md which reflects decrease in Radiant exposure fractal dimension from 2.7748 to 2.4379 as quantified in table 1. Again, an increase in grain size and permeability was proved from sample SJ4 whose Radiant exposure fractal dimension and capillary pressure fractal dimension was found to be 2.6843 as described in Table 1.

Figure 1. Surface type section of the Shajara Reservoirs of the Permo-Carboniferous Shajara Formation at latitude 26° 52' 17.4" longitude 43° 36' 18"

AGE	Fm.	Mbr.	unit	LITHO-LOGY	DESCRIPTION	
Late Permian	Khuff Formation	Huqayf Member			Limestone : Cream, dense, burrowed, thickness 6.56'	
					Sub-Khuff unconformity.	
Late Carboniferous - Permian	Shajara Formation	Upper Shajara Member	Upper Shajara mudstone		Mudstone : Yellow, thickness 17.7'	
				Upper Shajara Reservoir	SJ13▲ SJ12▲	Sandstone : Light brown, cross-bedded, coarse-grained, poorly sorted, porous, friable, thickness 6.5'
			Middle Shajara Member	Upper Shajara Reservoir	SJ11▲	Sandstone : Yellow, medium-grained, very coarse-grained, poorly, moderately sorted, porous, friable, thickness 13.1'
					Middle Shajara mudstone	
				Middle Shajara Reservoir		Mudstone : Yellow, thickness 1.3'
						Mudstone : Brown, thickness 4.5'
		Lower Shajara Member	Lower Shajara Reservoir	SJ10▲	Sandstone : Light brown, medium-grained, moderately sorted, porous, friable, thickness 3.6'	
				SJ9▲ SJ8▲	Sandstone : Yellow, medium-grained, moderately well sorted, porous, friable, thickness 0.9'	
				SJ7▲	Sandstone : Red, coarse-grained, medium-grained, moderately well sorted, porous, friable, thickness 13.4'	
				SJ6▲	Sandstone : White with yellow spots, fine-grained, hard, thickness 2.6'	
				SJ5▲ SJ4▲	Sandstone : Limonite, thickness 1.3' Sandstone : White, coarse-grained, very poorly sorted, thickness 4.5'	
		Lower Shajara Reservoir	SJ3▲ SJ2▲	Sandstone : White-pink, poorly sorted, thickness 1.6' Sandstone : Yellow, medium-grained, well sorted, porous, friable, thickness 3.9'		
			SJ1▲	Sandstone : Red, medium-grained, moderately well sorted, porous, friable, thickness 11.8'		
			Sub-Unayzah unconformity.			
		Early Devonian	Tawil Formation			Sandstone : White, fine-grained.

SJ1 ▲ Samples Collection

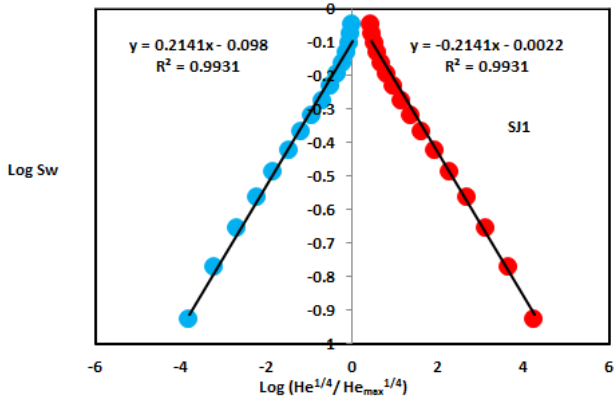


Figure 2. $\text{Log} (\text{He}^{1/4}/\text{He}_{\text{max}}^{1/4})$ & log pc versus log Sw for sample SJ1

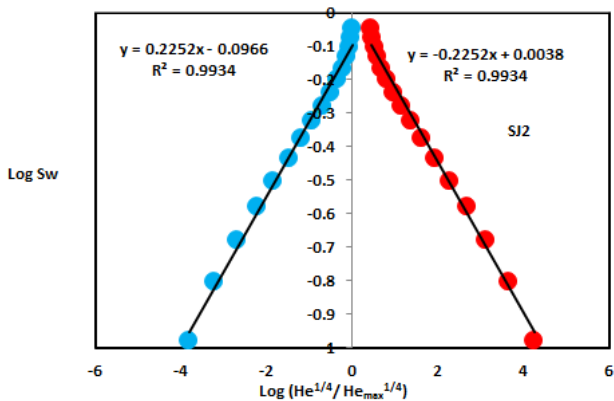


Figure 3. $\text{Log} (\text{He}^{1/4}/\text{He}_{\text{max}}^{1/4})$ & log pc versus log Sw for sample SJ2

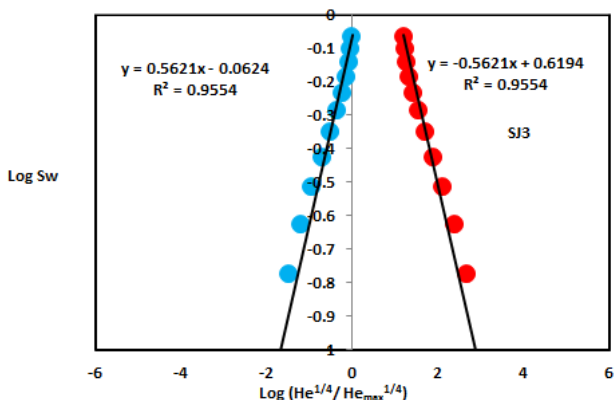


Figure 4. $\text{Log} (\text{He}^{1/4}/\text{He}_{\text{max}}^{1/4})$ & log pc versus log Sw for sample SJ3

In contrast, the Middle Shajara reservoir which is separated from the Lower Shajara reservoir by an unconformity surface as revealed in Figure 1. It was nominated by four samples (Figure 1), three of which named as SJ7, SJ8, and SJ9 as illuminated in Table1 were chosen for capillary measurements as described in Table 1. Their positive slopes of the first procedure and negative slopes of the second procedure are shown in Figure 6, Figure 7 and Figure 8 and Table 1. Furthermore, their Radiant exposure

fractal dimensions and capillary pressure fractal dimensions show similarities as defined in Table 1. Their fractal dimensions are higher than those of samples SJ3 and SJ4 from the Lower Shajara Reservoir due to an increase in their permeability as explained in table 1.

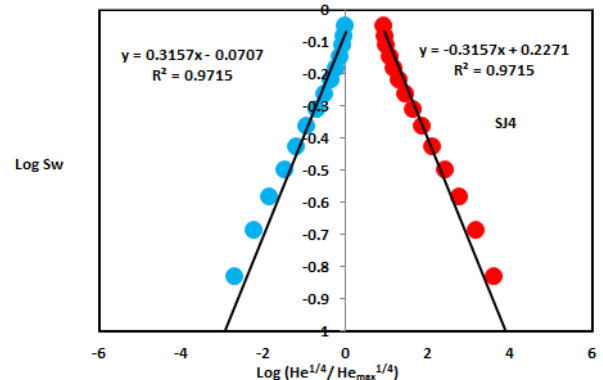


Figure 5. $\text{Log} (\text{He}^{1/4}/\text{He}_{\text{max}}^{1/4})$ & log pc versus log Sw for sample SJ4

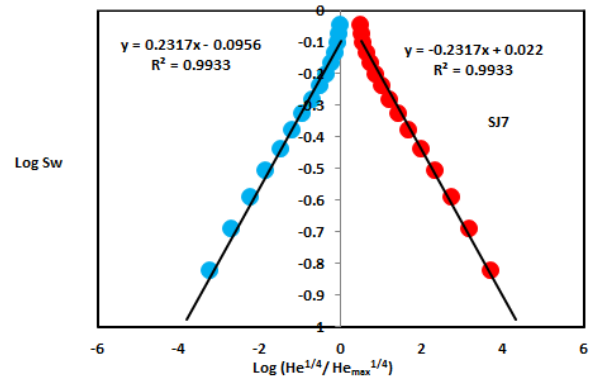


Figure 6. $\text{Log} (\text{He}^{1/4}/\text{He}_{\text{max}}^{1/4})$ & log pc versus log Sw for sample SJ7

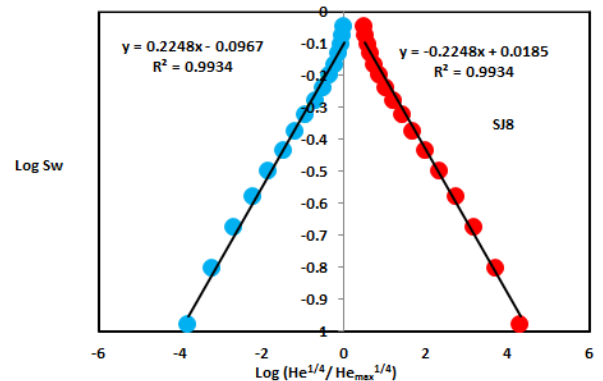


Figure 7. $\text{Log} (\text{He}^{1/4}/\text{He}_{\text{max}}^{1/4})$ & log pc versus log Sw for sample SJ8

On the other hand, the Upper Shajara reservoir was separated from the Middle Shajara reservoir by yellow green mudstone as shown in Figure 1. It is defined by three samples so called SJ11, SJ12, SJ13 as explained in Table 1. Their positive slopes of the first procedure and negative slopes of the second procedure are

displayed in Figure 9, Figure 10 and Figure 11 and Table 1. Moreover, their Radiant exposure fractal dimension and capillary pressure fractal dimension are also higher than those of sample SJ3 and SJ4 from the Lower Shajara Reservoir due to an increase in their permeability as simplified in table 1.

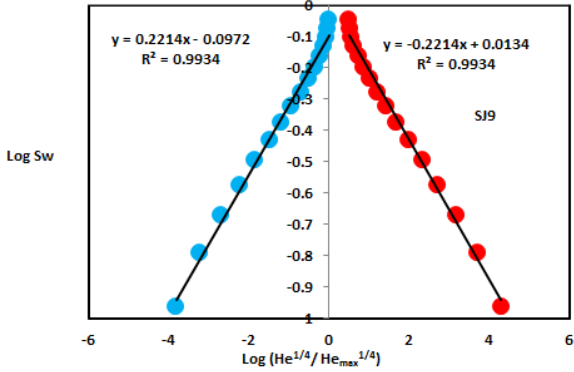


Figure 8. Log (He^{1/4}/He^{1/4}_{max}) & log pc versus log Sw for sample SJ9

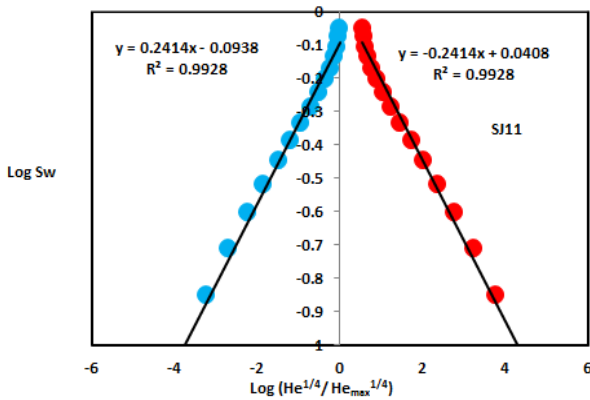


Figure 9. Log (He^{1/4}/He^{1/4}_{max}) & log pc versus log Sw for sample SJ11

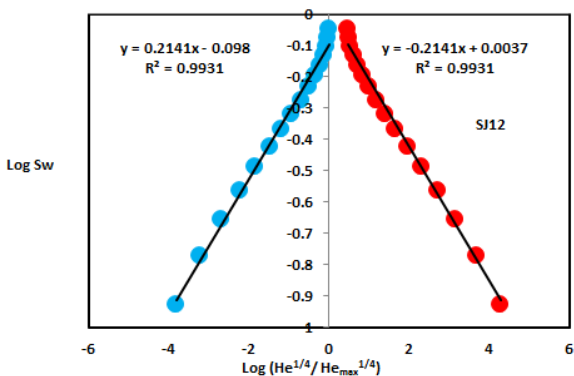


Figure 10. Log (He^{1/4}/He^{1/4}_{max}) & log pc versus log Sw for sample SJ12

Overall a plot of positive slope of the first procedure versus negative slope of the second procedure as described in Figure 12 reveals three permeable zones of varying Petrophysical properties. These reservoir zones were also confirmed by plotting Radiant

exposure fractal dimension versus capillary pressure fractal dimension as described in Figure 13. Such variation in fractal dimension can account for heterogeneity which is a key parameter in reservoir quality assessment.

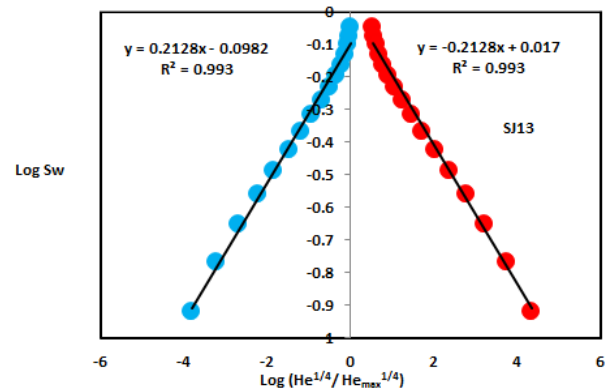


Figure 11. Log (He^{1/4}/He^{1/4}_{max}) & log pc versus log Sw for sample SJ13

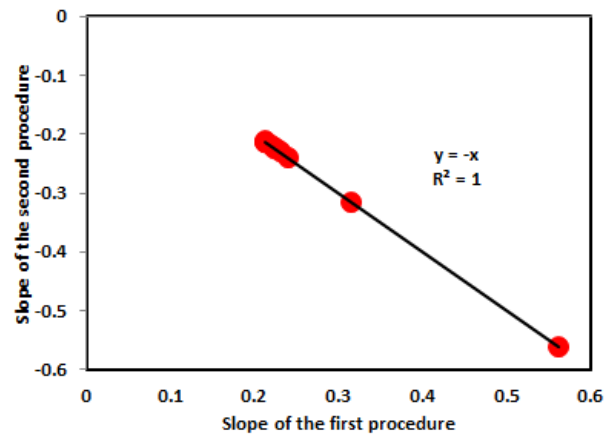


Figure 12. Slope of the first procedure versus slope of the second procedure

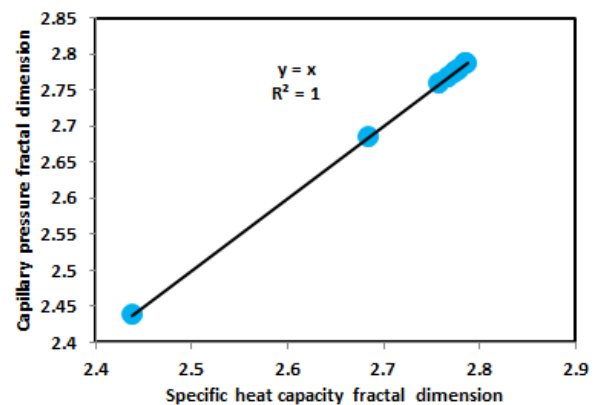


Figure 13. Radiant exposure fractal dimension versus capillary pressure fractal dimension

Conclusions

The sandstones of the Shajara Reservoirs of the permo-Carboniferous Shajara Formation were divided here into three units based on Radiant exposure fractal dimension. The Units from base

to top are: Lower Shajara Radiant Exposure Fractal Dimension Unit, Middle Shajara Radiant Exposure Fractal Dimension Unit, and Upper Shajara Radiant exposure Fractal Dimension Unit. These units were also proved by capillary pressure fractal dimension. The fractal dimension was found to increase with increasing grain size and permeability owing to possibility of having interconnected channels.

Acknowledgement

The author would to thank King Saud University, college of Engineering, Department of Petroleum and Natural Gas Engineering, Department of Chemical Engineering, Research Centre at College of Engineering, College of science, Department of Geology, and King Abdullah Institute for research and Consulting Studies for their supports.

Conflict of interest

Authors have declared that no conflict interest.

References

- [1] Frenkel J. On the theory of seismic and seismoelectric phenomena in a moist soil. *Journal of Physics* 1944;3(4):230-41.
- [2] Li K, Williams W. Determination of capillary pressure function from resistivity data. *Transport in Porous Media* 2007;67(1):1-15.
- [3] Revil A, Jardani A. Seismoelectric response of heavy oil reservoirs: theory and numerical modelling. *Geophysical Journal International* 2010; 180(2):781-97.
- [4] Dukhin A, Goetz P, Thommes M. Seismoelectric effect: a non-isochoric streaming current.1 Experiment. *Journal of Colloid Interface Science* 2010;345(2): 547-53.
- [5] Guan W, Hu H, Wang Z. Permeability inversion from low-frequency seismoelectric logs in fluid- saturated porous formations. *Geophysical Prospecting* 2012;61(1):120-33.
- [6] Hu H, Guan W, Zhao W. Theoretical studies of permeability inversion from seismoelectric logs. *Geophysical Research Abstracts* 2012;14.
- [7] Borde C., S´en´echal P, Barri`ere J. et al. Impact of water saturation on seismoelectric transfer functions: a laboratory study of co-seismic phenomenon. *Geophysical Journal International* 2015; 200(3):1317-1335.
- [8] Jardani A, Revil A. Seismoelectric couplings in a poroelastic material containing two immiscible fluid phases. *Geophysical Journal International* 2015; 202(2):850-70.
- [9] Holzhauer J, Brito D, Bordes C, Brun Y, Guatarbes B. Experimental quantification of the seismoelectric transfer function and its dependence on conductivity and saturation in loose sand. *Geophysical Prospecting* 2016;65:1097-120.
- [10] Ping R, Wei J-X, Di B-R, Ding P-B, Liu Z-C. Experimental research on seismoelectric effects in sandstone. *Applied Geophysics* 2016;13:425-36.
- [11] Djuraev U, Jufar SR, Vasant. P. Numerical Study of frequency-dependent seismo electric coupling in partially-saturated porous media. *MATEC Web of Conferences* 87, 02001 (2017).
- [12] Alkhidir KEME. Pressure head fractal dimension for characterizing Shajara Reservoirs of the Shajara Formation of the Permo-Carboniferous Unayzah Group, Saudi Arabia. *Archives of Petroleum and Environmental Biotechnology* 2017; 2:1-7.
- [13] Al-Khidir KE. On Similarity of Pressure Head and Bubble Pressure Fractal Dimensions for Characterizing Permo-Carboniferous Shajara Formation, Saudi Arabia. *Journal of Industrial Pollution and Toxicity* 2018;1(1):1-10.
- [14] Alkhidir KEME. Geometric relaxation time of induced polarization fractal dimension for characterizing Shajara Reservoirs of the Shajara Formation of the Permo-Carboniferous Unayzah Group, Saudi Arabia. *Scifed Journal of Petroleum* 2018;2(1):1-6.
- [15] Alkhidir KEME. Geometric relaxation time of induced polarization fractal dimension for characterizing Shajara Reservoirs of the Shajara formation of the Permo-Carboniferous Unayzah Group-Permo. *International Journal of Petrochemistry and Research* 2018;2(1):105-8.
